



Contents lists available at ScienceDirect

## Deep-Sea Research I

journal homepage: [www.elsevier.com/locate/dsr](http://www.elsevier.com/locate/dsr)

# The deep-water motion through the Lifamatola Passage and its contribution to the Indonesian throughflow

Hendrik M. van Aken<sup>a,\*</sup>, Irsan S. Brodjonegoro<sup>b</sup>, Indra Jaya<sup>c</sup>

<sup>a</sup> NIOZ Royal Netherlands Institute for Sea Research, Texel, The Netherlands

<sup>b</sup> ITB Institute of Technology Bandung, Bandung, Indonesia

<sup>c</sup> IPB Bogor Agricultural University, Indonesia

## ARTICLE INFO

### Article history:

Received 28 August 2008

Received in revised form

26 January 2009

Accepted 1 February 2009

Available online 7 February 2009

### Keywords:

Indonesian throughflow

INSTANT

Lifamatola Passage

Current measurements

## ABSTRACT

In order to estimate the contribution of cold Pacific deep water to the Indonesian throughflow (ITF) and the flushing of the deep Banda Sea, a current meter mooring has been deployed for nearly 3 years on the sill in the Lifamatola Passage as part of the International Nusantara Stratification and Transport (INSTANT) programme. The velocity, temperature, and salinity data, obtained from the mooring, reflect vigorous horizontal and vertical motion in the lowest 500 m over the ~2000 m deep sill, with speeds regularly surpassing 100 cm/s. The strong residual flow over the sill in the passage and internal, mainly diurnal, tides contribute to this bottom intensified motion. The average volume transport of the deep throughflow from the Maluku Sea to the Seram Sea below 1250 m is 2.5 Sv ( $1 \text{ Sv} = 10^6 \text{ m}^3/\text{s}$ ), with a transport-weighted mean temperature of 3.2 °C. This result considerably increases existing estimates of the inflow of the ITF into the Indonesian seas by about 25% and lowers the total mean inflow temperature of the ITF to below 13 °C. At shallower levels, between 1250 m and the sea surface, the flow is directed towards the Maluku Sea, north of the passage. The typical residual velocities in this layer are low (~3 cm/s), contributing to an estimated northward flow of 0.9–1.3 Sv. When more results from the INSTANT programme for the other Indonesian passages become available, a strongly improved estimate of the mass and heat budget of the ITF becomes feasible.

© 2009 Elsevier Ltd. All rights reserved.

## 1. Introduction

In his description of the warm return flow of the thermohaline overturning circulation, Gordon (1986) stressed that interocean exchange of thermocline waters is an essential process to maintain this density-driven global circulation system. One of the important exchange processes is the Indonesian throughflow (ITF), which transports water from the low latitude Pacific Ocean through the Indonesian seas to the eastern Indian Ocean.

Gordon (1986) assumed that in the ITF about 8.5 Sv ( $1 \text{ Sv} = 10^6 \text{ m}^3/\text{s}$ ) flows in the upper 1000 m through several branches in the Indonesian seas, while diapycnal mixing in the ITF maintains a local downward air–sea heat exchange of about 100 W/m<sup>2</sup>. Simulations with ocean general circulation models as well as with coupled global climate models have shown that the existence of the ITF has far-reaching consequences for the global ocean circulation and climate (e.g. Schneider, 1998; Wajsovicz and Schneider, 2001; Pandey et al., 2007).

Hydrographic observations (temperature, salinity, CFCs) have shown that this shallow inflow into the Indonesian seas (full arrows in Fig. 1) occurs mainly through the Makassar Strait between the islands Kalimantan and Sulawesi (Gordon and Fine, 1996). The shallow Dewakan

\* Corresponding author.

E-mail addresses: [aken@nioz.nl](mailto:aken@nioz.nl) (H.M. van Aken), [irsansb@ocean.itb.ac.id](mailto:irsansb@ocean.itb.ac.id) (I.S. Brodjonegoro), [indrajaya@ipb.ac.id](mailto:indrajaya@ipb.ac.id) (I. Jaya).

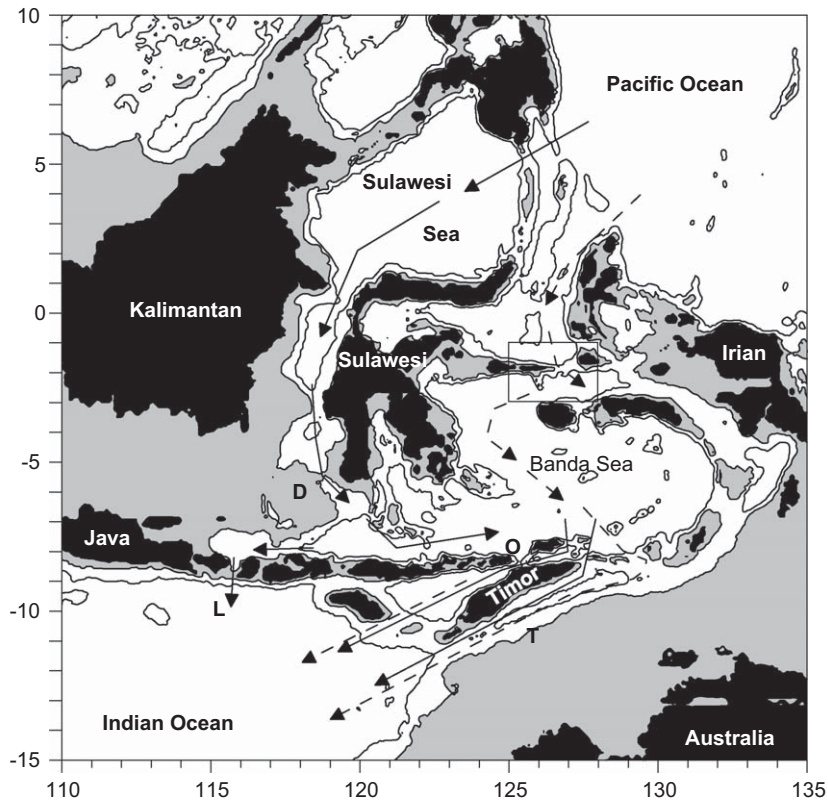


**Fig. 1.** Map of the Indonesian throughflow. The full arrows depict the main shallow throughflow route via Makassar Strait. The dashed arrows show the deep throughflow from the Pacific Ocean via the Banda Sea to the Indian Ocean. The full line shows the 2000-m isobath, while the shaded area is shallower than 500 m. The area in the rectangle encompasses the Lifamatola Passage and is enlarged in Fig. 2. The capitals D, L, O, and T indicate the approximate locations of, respectively, the Dewakan sill, Lombok Strait, Ombai Strait, and Timor Passage.

sill at the southern end of Makassar Strait (D in Fig. 1) has a sill depth of about 680 m (Gordon et al., 2003b). Current measurements in Makassar Strait have shown that the throughflow through Makassar Strait is about 10 Sv, with a maximum contribution from the layer between 150 and 200 m (Gordon et al., 1999, 2003a). The mean temperature of the throughflow in Makassar Strait is nearly 15 °C (Vranes et al., 2002; Gordon et al., 2003a). The main exits of the ITF towards the Indian Ocean are the passages between the lesser Sunda Islands (Nusantara), in particular Lombok Strait, Ombai Strait, and Timor Passage (L, O, and T in Fig. 1, respectively).

Because of the limited depth of the Dewakan sill in Makassar Strait, ventilation of the deep basins in the Banda Sea, with depths in the Weber Deep surpassing 7000 m, requires another pathway. Van Riel (1956) derived, from the changing temperature stratification measured during the Snellius Expedition in 1929–1930, that the flushing of the deep Banda Sea follows a pathway from the Pacific Ocean, via the Lifamatola Passage east of Sulawesi (box in Fig. 1, and Fig. 2). The sill in this passage has a depth between 1900 and 2000 m (van Riel, 1956; Broecker et al., 1986), allowing a deep throughflow with temperatures well below that of the throughflow in Makassar Strait. Van Aken et al. (1988) and Gordon et al. (2003b) have shown, from tracer distributions, that the

hydrographic stratification in the deep Banda Sea agrees with a ventilation by deep overflow from the Pacific Ocean via the Lifamatola Passage. Thereby the cold throughflow water descends from the Lifamatola sill along the topography in an approximately 500 m thick layer, first into the 5000 m deep Seram Sea, and second from the Seram Sea over a 3500 m deep sill into the Banda Sea (Van Aken et al., 1988). Along this path some heating of the bottom water is observed, mainly attributed to mixing with warmer overlying water near the sills (Van Aken et al., 1988). Consequent deep upwelling and mixing in the Banda Sea then brings the deep throughflow water from a depth of 5000 to about 1000 m (Van Aken et al., 1991; Gordon et al., 2003b). Above the latter level the water from the deep throughflow leaves the Banda Sea towards the Indian Ocean through the southern exits, joining the shallow throughflow water from Makassar Strait over the 680 m deep Dewakan sill.

Direct measurements of the flow across the sill in the Lifamatola Passage and subsequent transport estimates are scarce. Over 70 years ago Lek (1938) carried out observations with an Ekman current meter at an anchor station of the RV Snellius which lasted less than 35 h. At 1500 m he found a mean southeastward flow of about 5 cm/s. He also observed strong internal semidiurnal and diurnal tides, with amplitudes reaching over, respectively,

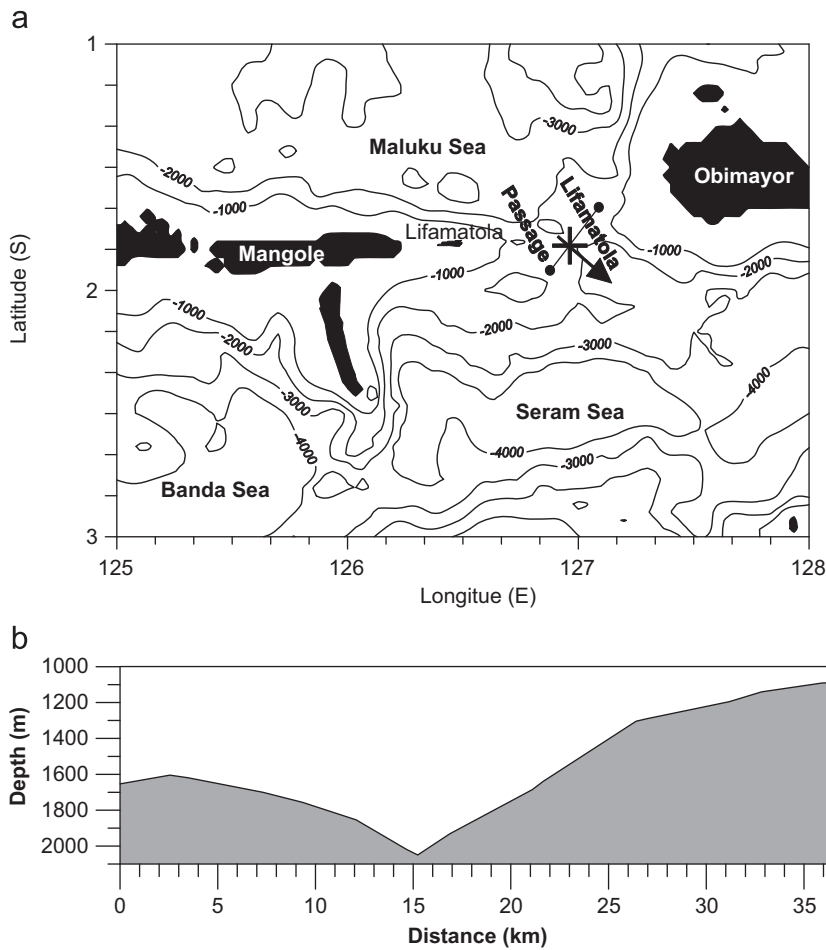


**Fig. 2.** Plot of the topography near the Lifamatola Passage, between the small Lifamatola Island and the larger island Obimayor, with isobaths every 1000 m (a), based on the Smith and Sandwell (1997)  $2' \times 2'$  resolution ETOPO-2 topographic data set. The cross indicates the position of the current meter mooring near the sill of the passage, while the arrow in the direction  $129^\circ$  shows the observed mean current direction in the lowest 500 m. The line, perpendicular to the vector, ending in dots, is the cross-section for which transports have been calculated. The bottom profile along this line is shown in (b). The mooring was located at  $x = 14.7$  km.

30 and 15 cm/s at several depths. Broecker et al. (1986) reported observations with two self-recording current meters over the sill, each about 10 m above the bottom, which lasted 28 days. They found a typical steady southeastward residual velocity of about 25 cm/s, in agreement with a deep flow of Pacific water towards the Banda Sea. This flow was modified by weaker ( $\sim 10$  cm/s) diurnal and semidiurnal tides. Van Aken et al. (1988) reported 3.5 months of current measurements with a current meter mooring over the sill. At 60 m above the bottom the mean velocity was 61 cm/s, directed to the southeast, while at 200 m above the sill the mean velocity was 40 cm/s, in the same direction. Superimposed on the mean residual flow were tidal motions of a mixed semidiurnal and diurnal character, leading to total velocities in the bottom layer that regularly surpassed 1 m/s. From these current measurements the deep inflow below 1500 m was estimated to be 1.5 Sv. Luick and Cresswell (2001) carried out observations with a single current meter mooring, located at  $1^\circ 41' N$ , nearly 400 km

north of the Lifamatola Passage, in a 230 km wide passage of the Maluku Sea east of Sulawesi. Assuming a horizontally homogenous flow, they reported a southward transport between 740 and 1500 m of 7 Sv. However, one can question whether a single observational point can be representative for the ocean circulation in that 230 km wide passage, especially since the hydrographic observations ( $T$ ,  $S$ ,  $O_2$ ) indicate the presence of a cyclonic circulation in the Maluku Sea below 1800 m (Luick and Cresswell, 2001).

Several research programmes have aimed at the direct measurement of the other branches of the ITF, both in Makassar Strait (Gordon et al., 1999, 2003a) and in the southern exit channels (Murray and Arief, 1988; Molcard et al., 1994, 1996, 2001). However, the observations from those experiments do not supply a contemporaneous data set of the ITF, since the experiments were carried out in different years. Therefore, the average structure and magnitude of the total transport of mass, heat, and freshwater by the ITF are not well known. This lack of

information hampers the validation of ocean general circulation models and global climate models. In response to this lack of knowledge the International Nusantara Stratification and Transport (INSTANT) programme was established to directly and simultaneously measure the ITF, both in the northern inflow passages and in the southern outflow passages (Sprintall et al., 2004). In this international research programme, scientists from Indonesia, the USA, Australia, France, and the Netherlands cooperated to determine the strength of the ITF entering and leaving the Indonesian seas during three consecutive years. Variations in the ITF will be related to changes in the meteorological and oceanographic forcing (sea level, monsoons, El Niño, Indian Ocean Dipole, etc.). This paper deals with the observations with a current meter mooring over the sill in Lifamatola Passage, carried out during the INSTANT programme. It mainly focuses on the through-flow of the Lifamatola Passage and its variability, but also describes the higher-frequency (tidal) current oscillations in the passage.

## 2. The data

The sill depth in Lifamatola Passage is about 2000 m (Fig. 2). Slightly downstream of the sill a mooring was deployed twice for a period of about 1.5 years, leading to a total mooring period of over 34 months (Table 1). The deployment cruise in January 2004, the service cruise in

July 2005, and the recovery cruise in January 2006 were all carried out with the Indonesian RV Baruna Jaya I. During these cruises, series of CTD casts were also recorded, with during each cruise at least one CTD cast close to the mooring position, reaching from the sea surface to the bottom. For the first period the mooring was fitted with two RDI 75 kHz ADCPs (Long Ranger), covering the upper and lower parts of the water column, upward looking near the surface, and downward looking in the bottom layer. At intermediate levels, three Aanderaa RCM 11 acoustic current meters were mounted. All RDI and Aanderaa instruments were fitted with a tilt sensor for the correction of the velocity, measured from a tilted mooring. Each of these instruments contained a temperature sensor, while the ADCPs were also fitted with a pressure sensor. Additionally five Sea Bird Electronics Microcats (SBE37SM) were mounted to record pressure, temperature, and salinity (Table 1). The mooring position appeared to be about 30 m shallower than the deepest part of the nearby deep channel over the sill, at a distance of about 1 km further northeast. After recovery of this mooring it appeared that because of a faulty but undocumented setting of these instruments, only 7 of the 80 data bins of 8 m length were recorded, strongly diminishing the information on the ITF, which is assumed to be concentrated in the near-surface and near-bottom layers. Moreover, it appeared that because of very strong tides the 15-min average velocity at mid-levels regularly surpassed 140 cm/s. This caused a serious blow-down of

**Table 1**  
Description of the INSTANT moorings in the Lifamatola Passage.

Mooring name	Latitude	Longitude	Deployment date	Recovery date	Corrected depth (m)
LOCO-10-1	1°49.1'N	126°57.8'E	26-01-2004	17-07-2005	2019
Height above bottom (m)	Instrument type	Serial number	Sampling interval (min)		
1535	RDI ADCP	3553	30		
1534	SBE 37 Microcat	2672	5		
1232	Aanderaa RCM 11	243	15		
1231	SBE 37 Microcat	2673	5		
931	Aanderaa RCM 11	244	15		
930	SBE 37 Microcat	2674	5		
630	Aanderaa RCM 11	245	15		
613	SBE 37 Microcat	2659	5		
608	RDI ADCP	3714	30		
10	SBE 37 Microcat	2961	No data		
Mooring name	Latitude	Longitude	Deployment date	Recovery date	Corrected depth (m)
LOCO-10-2	1°49.1'N	126°57.8'E	17-07-2005	04-12-2006	2017
Height above bottom (m)	Instrument type	Serial number	Sampling interval (min)		
1233	RDI ADCP	3553	30		
1231	SBE 37 Microcat	2959	5		
931	Aanderaa RCM 11	403	15		
930	SBE 37 Microcat	2672	5		
630	Aanderaa RCM 11	243	15		
613	SBE 37 Microcat	4139	5		
608	RDI ADCP	3714	5		
10	SBE 37 Microcat	2674	30		

the mooring with an average range of 435 m, adding to the information loss. In the second deployment period the mooring was shortened by 300 m to reduce blow-down, which decreased to an average range of 252 m. However, thereby the possibility to measure velocity in the upper 300 m was lost. The faulty ADCP setting was also repaired, so that effectively in the second period our information on the current structure covered a larger part of the water column, although data reached only to 300 m below the sea surface. The bias in the horizontal velocity, induced by the horizontal motion of the sensors due to the blow-down, was estimated to be about 2 cm/s or less, with a periodic character. Since the focus of this paper is on the throughflow, and since the dominant tides have an amplitude of at least an order of magnitude larger, this bias has been ignored.

After recovery of the moorings, the recorded directions were corrected for the magnetic variation, and, by a combination of low-pass filtering (filter width  $\approx 1/h$ ) and sub-sampling every whole hour, a synchronous hourly data set for all sensors and ADCP bins was produced, including sensor or bin depth. A shift of the time base of each instrument was applied in this process to correct for the effects of different recording intervals and the different meanings of the time stamps in the different instruments (beginning, centre, or end of the recording interval). From these synchronized and depth-dependent data, time series of hourly data were calculated at fixed depth levels by means of vertical linear interpolation, every 100 m in the upper 1600 m and every 50 m from 1600 to 2000 m. Continuous hourly data records are available for the interpolation depth interval from 1000 to 1500 m in the first deployment period, and for the 1000–2000 m depth interval in the second deployment period. In order to recover information on the low-frequency flow in the parts of the water column where data were available only for part of the tidal period because of the mooring blow-down, the monthly mean

residual current was estimated from a harmonic analysis with the dominant tidal frequencies (see below). For the first deployment period this supplied us with monthly mean residual current data from 500 to 1800 m, and for the second period from 300 to 2000 m.

From the average current components between 1500 and 2000 m, measured during the second deployment period, the mean deep current direction was determined to be  $129^\circ$  (arrow in Fig. 2). This direction appears to be well aligned with the deep channel over the sill. In the following discussion we have rotated our geographic reference frame, naming the direction  $129^\circ$  along-channel, and the direction perpendicular to the channel,  $219^\circ$ , cross-channel.

### 3. The character of the currents and their variability

Current data at 1500 m are available for the whole deployment period (Fig. 3). At this level the mean velocity is 14.7 cm/s to the southeast ( $119^\circ$ ). The magnitudes of the temporal variation of the current components, expressed as standard deviation, are 20.7 and 17.5 cm/s for, respectively, the east and north components. The plot of both velocity components (Fig. 3) shows a considerable contribution from the tides, with an envelope that shows more or less regular fortnightly variability, indicative of the spring tide–neap tide phenomenon, as well as longer-term changes of the residual flow. At 1500 m the tides cause a regular reversal of the current direction. This tidal reversal of the current direction is observed even during spring tide at 2000 m, about 20 m above the bottom. However, during neap tide the residual current at 2000 m is larger than the tidal contribution, maintaining a permanent southeastward bottom flow. During 0.16% of the 1-h data records the current speed at 1500 m exceeds 1 m/s. This fraction increases to 12.6% at 2000 m. Variability at lower frequencies can be observed in the background,

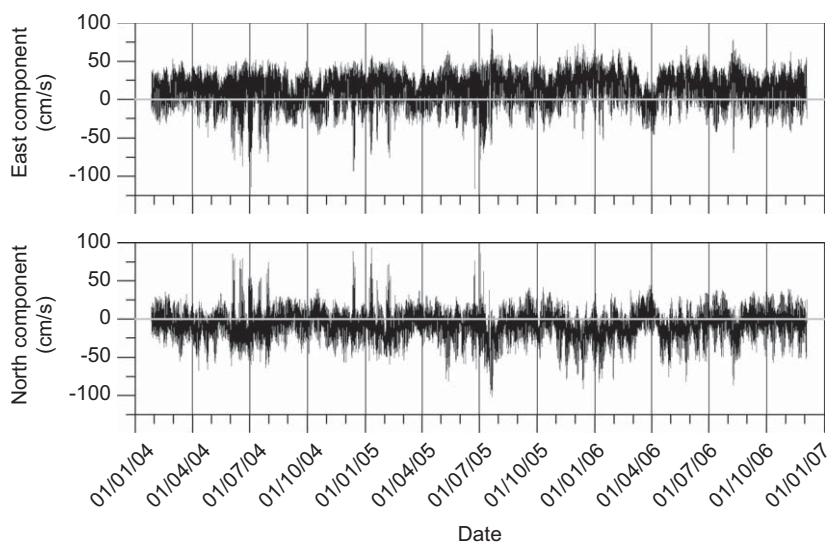
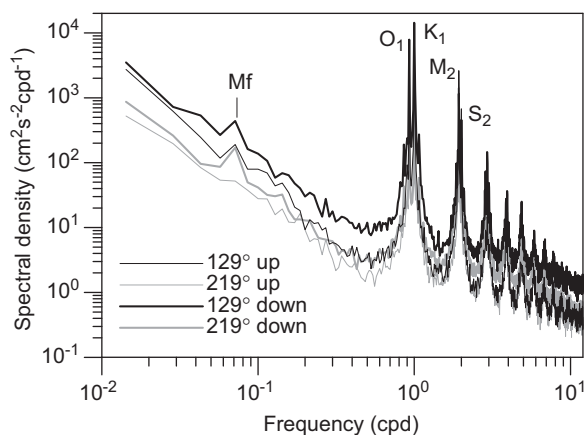


Fig. 3. Time series of the hourly current components at a depth of 1500 m for both deployment periods combined.

leading, for example, to a reversal of the low-pass flow direction at 1500 m during the weeks around 1 April 2006.

The rotary spectrum (not shown) has characteristic tidal bands centred around about  $N$  cpd (cycle per day),  $N$  being an integer number between 1 and 12. Analysis of the anisotropy of these tidal bands of rotary spectra at the interpolation depths has shown that apart from the semidiurnal tidal bands at 1500 m the variable currents at tidal frequencies are mainly linearly polarized. The characteristic amplitudes of the anti-clockwise (ACW) and clockwise (CW) components for those tidal bands were all of the same order of magnitude with ratios ACW/CW varying between 0.7 and 1.4, on average  $1.0 (\pm 0.1 \text{ stdev})$ . As a single exception more extreme values of the ACW/CW ratios were found only in the semidiurnal band at 1500 m, where the ACW/CW ratio was 2.7, indicative of the dominance of ACW motion at this depth in this frequency band. This suggests a large influence of the topography on other frequencies and at deeper levels in the channel over the sill. The tidal currents below 1500 m were all aligned in the along-channel direction.

The layer-averaged power spectra for the along-channel and cross-channel velocity (Fig. 4) confirm the conclusion, presented by Van Aken et al. (1988), that the tidal current in the Lifamatola Passage is dominated by the diurnal ( $O_1$  and  $K_1$ ) and semidiurnal ( $M_2$  and  $S_2$ ) frequencies, while additional peaks are found at their higher harmonics, at  $\sim N$  cpd ( $N = 3, 4, 5, \dots$ ). Additionally, a spectral peak is found near the lunar fortnightly (Mf) frequency ( $7.32 \times 10^{-2}$  cpd). The latter is close to, but not coincident with, the local inertial frequency of  $6.37 \times 10^{-2}$  cpd. The difference of the spectra for the along-channel and cross-channel components shows that in the depth interval from 1600 to 2000 m, completely surrounded by the channel wall (thick lines in Fig. 4), the kinetic energy



**Fig. 4.** Power spectrum of the velocity components in along-channel (129°, black lines) and cross-channel (219°, grey lines) direction, averaged over the depth intervals 1000–1500 m (up, thin lines) and 1600–2000 m (down, thick). The peaks at the dominant semidiurnal and diurnal tidal component as well as the lunar fortnightly components are identified. These spectra are based on successive 70-day sub-periods during the second deployment period, with an overlap of 35 days.

of the along-channel velocity variations is on average 19 times the kinetic energy of the cross-channel variations at diurnal and semidiurnal frequencies. At the sub-diurnal frequencies below 0.5 cpd that ratio for the spectral continuum is about 3, at super-semidiurnal frequencies about 2.3. This anisotropy reflects the fact that over the sill the variable motion takes place in a narrow channel, 8.5 km wide at the depth of the 1800 m isobath, which hinders the cross-channel motion considerably. At the level from 1000 to 1500 m the channel is much wider (28 km at the 1250 m level), and consequently the anisotropy of the variable motion is smaller,  $\sim 5$  at the tidal peaks,  $\sim 2$  at sub-diurnal frequencies, and  $\sim 1.2$  at super-semidiurnal frequencies.

To show the character of the tides in more detail, a harmonic tidal analysis of the data has been carried out for the fortnightly, diurnal, and semidiurnal tides, indicated in Fig. 4, as well as for higher harmonics, up to at least  $\sim 6$  cpd tides. It appears that the strongest tides are, in order of amplitude,  $K_1$ ,  $O_1$ ,  $M_2$ ,  $S_2$ , and Mf, all five with amplitudes at all depths between 1000 and 2000 m of over 1 cm/s in the along-channel direction. The determination coefficient (correlation  $R$  squared) of the harmonic analysis shows that these five tidal frequencies determine on average 65% of the along-channel current variation ( $R = 0.80$ ). All the higher harmonics have amplitudes less than 1 cm/s. The tidal ellipses for the dominant frequencies (Fig. 5) confirm that the diurnal tides,  $K_1$  and  $O_1$ , are the strongest between 100 and 200 m above the bottom of the sill with along-channel amplitudes of, respectively, 33 and 25 cm/s. The narrow ellipses for  $K_1$  and  $O_1$  are fairly well aligned in the direction  $129^\circ$  of the deep channel of the Lifamatola Passage, decreasing upwards in amplitude. The phase shift from 1800 to 1200 m was about  $35^\circ$ . This suggests that these tides have the character of internal tides with an upward energy flux, generated on the slope below the sill by interaction of the barotropic tide with the sill topography in a stratified ocean (Gill, 1982). The rotation sense of the ellipses of the diurnal tides varies with depth, being anti-clockwise in the bottom layer below  $\sim 1900$  m, in an  $\sim 200$  m thick layers around 1400 m, and above 1100 m. In the other layer the rotation sense was clockwise. The ellipses for the semidiurnal tides and the lunar fortnightly tide are less narrow, and their orientation varies with depth, suggesting that these tides are propagated across the mooring site as internal waves from different generation areas. The rotation sense of the ellipses of these tidal components was dominantly anti-clockwise below 1200 m, turning to clockwise rotation above this depth level. The vertically varying rotation sense of the tidal ellipses shows that they do not behave as free waves in an infinite ocean, but interact with lateral walls (Gill, 1982). It is expected that the strong internal tides near narrow straits like the Lifamatola Passage support turbulent mixing, which contributes to the water mass transformation of the ITF water in the Indonesian seas (Ffield and Robertson, 2005; Koch-Larrouy et al., 2007). Local results of intense turbulent mixing for the temperature and oxygen distributions in the Lifamatola Passage have been described by Van Aken et al. (1988) and Tomczak and Godfrey (1994).

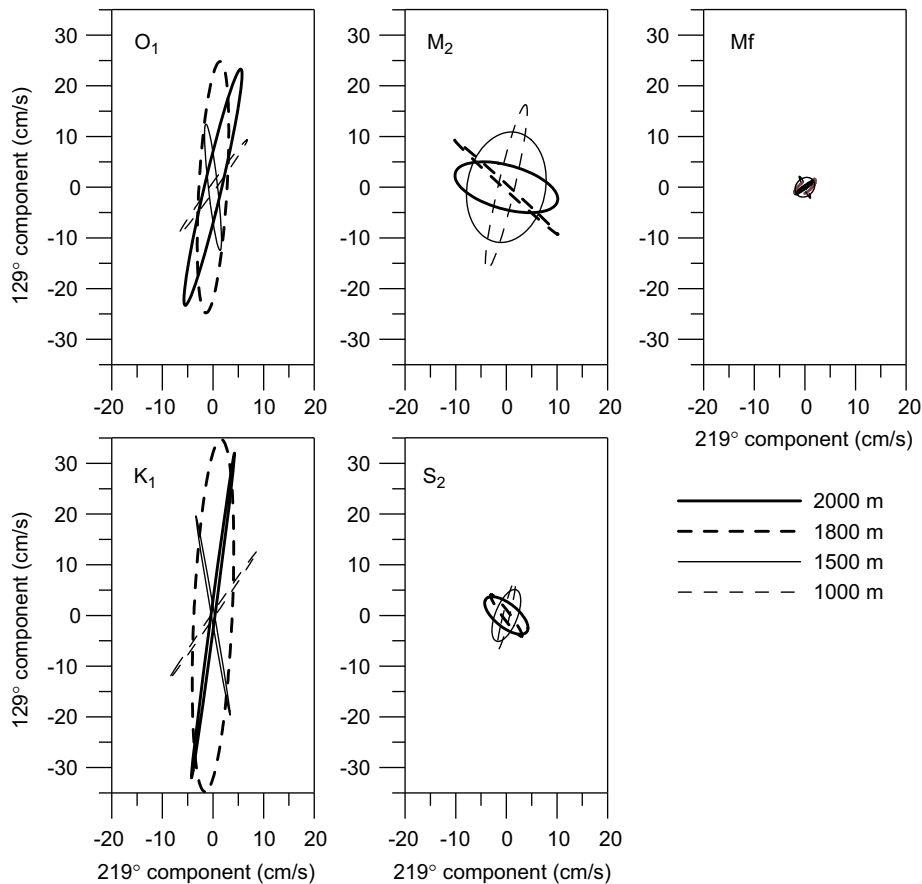


**Fig. 5.** Plots of the tidal ellipses at depths of 2000, 1800, 1500, and 1000 m for the tidal components  $O_1$ ,  $K_1$ ,  $M_2$ ,  $S_2$ , and  $M_f$ . These ellipses were determined with a harmonic analysis of the depth-interpolated current data from the second deployment period.

#### 4. The mean current profile

For the first deployment period uninterrupted interpolated hourly velocity data are available for the depth interval of 1000–1500 m, for the second deployment period from 1000 to 2000 m. Only for these depth intervals can the residual currents be determined directly by averaging of the hourly data. To extend the information on the residual currents further in the vertical, we have applied an alternative method. As shown above, most of the current variability comes from only five tidal components plus sub-tidal variability with time scales from months to years. Assuming that the along-channel current can be described quite well as a monthly mean residual current plus tidal contributions from the  $O_1$ ,  $K_1$ ,  $M_2$ ,  $S_2$ , and  $M_f$  components, harmonic analysis by means of multiple linear regression (Emery and Thomson, 1997) can be used to estimate the monthly mean along-channel current components. This can also be applied to those parts of the water column where, because of the blow-down of the moorings, the current record is not continuous, but interrupted by short periods of missing data. This has allowed us to extend the mean current profiles, based on monthly averages of the residual velocity, for the first deployment period to the depth interval from 500 to

1700 m, and for the second deployment period from 300 to 2000 m.

The current profiles for the two different deployment periods, derived from the monthly mean residual currents (grey lines in Fig. 6), are quite similar to each other. The resulting long-term averaged current profile (black line with symbols in Fig. 6) shows a strong southeastward overflow in the lowest 750 m over the sill, following the axis of the channel. From 300 to 1200 m a small but significant northwestward flow of about  $3.2 (\pm 0.5 \text{ stderr})$  cm/s is observed. In the deep overflow the average along-channel velocity reaches a maximum of  $67 (\pm 6 \text{ stderr})$  cm/s at 1950 m, about 70 m above the bottom, decreasing downwards to 51 cm/s at 2000 m.

The historic current estimates, discussed in the introduction (crosses in Fig. 6), compare reasonably well in order of magnitude and vertical structure with our averaged current profile, especially if we consider their limited accuracy and much different observational periods. On average these estimates are 62% of our mean currents at similar depths. The relatively low near-bottom velocities reported by Broecker et al. (1986) agree with the downward velocity decrease that we observe below 1950 m, especially considering that the velocities were measured at 10 m above the bottom, while our lowest

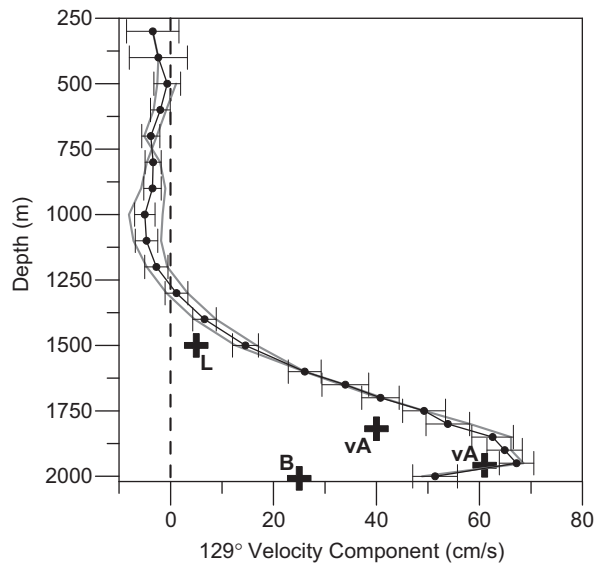


**Fig. 6.** Mean profile of the along-channel current component ( $129^\circ$ , black line with symbols) and estimated accuracy (twice the standard error), derived from monthly mean values, with separate curves (grey lines) for the first and second deployment periods. The crosses show mean velocities from the literature, shifted vertically to the appropriate distance from the bottom (L = Lek, 1938; B = Broecker et al., 1986; vA = Van Aken et al., 1988).

profile level at 2000 m was about 20 m above the bottom. The information available from our current profile shows that the southeastward deep overflow extends from the bottom to a depth of about 1250 m, while Van Aken et al. (1988), with data from only two current meters, derived from extrapolation a current reversal at 1500 m. Their averaged velocities were also smaller than those presented here. Therefore it can be expected that the average transport in the deep overflow presented here is larger than their estimate of 1.5 Sv.

## 5. The temperature and salinity stratification

The depth over which the temperature sensors in the mooring moved, because of the blow-down of the mooring, was in general of the same order of magnitude or larger than the expected vertical tidal migration of the isotherms of a few 100 m (Van Aken et al., 1988). Therefore, enough observations were available in the water column between 500 and 2000 m to determine the long-term ( $\sim 3$  years) mean profiles of potential temperature and salinity (Fig. 7). These show a salinity minimum at  $\sim 800$  m, where in the South Pacific Ocean a similar minimum is found (Wyrтки, 1961). In the lowest 400 m, where the core of the overflow of deep Pacific water into the Seram Sea/Banda Sea system is expected (Van Aken et al., 1988) the vertical gradient of salinity and potential temperature is larger than directly above this layer.

While during the first deployment period the near-bottom Microcat was defective, during the second deployment period this instrument recorded continuously the

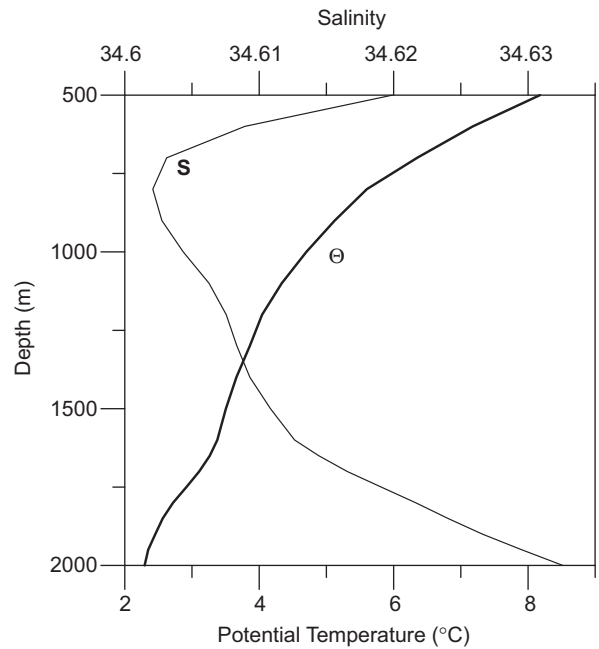


**Fig. 7.** Mean profiles of potential temperature (thick line) and salinity (thin line) between 500 and 2000 m, averaged over the whole deployment period.

near-bottom temperature and salinity in the lowest 10 m. Similar to the velocity signal, the temperature and salinity signals show a strong tidal variability (Fig. 8), with a clear fortnightly variation in amplitude. The temperature and salinity variations are negatively correlated as can be expected from the mean stratification with opposite  $\Theta$  and S gradients, depicted in Fig. 7. Therefore the tidal signals of these parameters are in opposite phase, with temperature maxima coinciding with salinity minima (Fig. 8). The spectra of temperature and salinity, derived from this time series (Fig. 9), clearly show the presence of the same dominant tides, which are also observed in the velocity spectrum, including the higher harmonics of the tides. The tidal character of these scalars is therefore also mixed diurnal and semidiurnal.

At sub-tidal frequencies some variation is still present in temperature and salinity. When we remove the tidal variability at fortnightly and shorter time scales with a 15-day running average, we can draw a time–depth diagram of the temperature, showing the temporal variability of the stratification at sub-tidal frequencies (Fig. 10). A deep maximum of the sub-tidal temperature variability is observed at 1750 m (stdev =  $0.14^\circ\text{C}$ ), nearly twice the variability 250 m higher or lower (stdev =  $0.08^\circ\text{C}$ ). Below 1200 m the depths of the isotherms show more variability at low frequencies than above this level. Over short vertical distances the correlation of the temperature in this deep layer is significant ( $p = 1\%$ ), being 0.79, 0.64, and 0.43 over vertical distances of, respectively, 50, 100, and 200 m. However, over larger vertical distances, e.g. 400 and 500 m, the correlation reduces to values of 0.10 and  $-0.02$ , while the correlation between the near-bottom temperature at 2000 m and the temperature at 1300 m

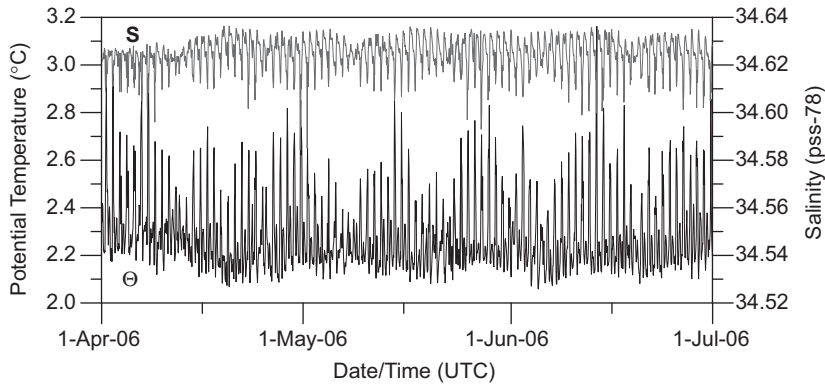


**Fig. 8.** Continuous plot of the near-bottom temperature (black line) and salinity (grey line), measured with an SBE Microcat for the sub-period April until June 2006.

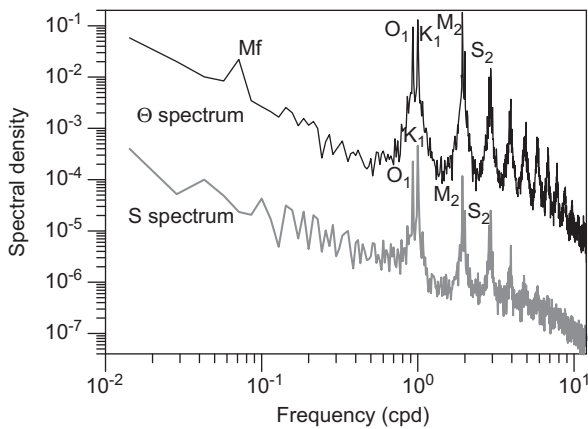


**Fig. 9.** Power spectra of the near-bottom temperature (black line) and salinity (grey line), measured with an SBE Microcat in the second deployment period.

has even a negative extreme of  $-0.27$ . The significant positive correlation is due to the apparent simultaneous upward or downward movements of thick layers of water with their isotherms, reflected by coincident upward or downward peaks in the isotherms (Fig. 10). However, at larger vertical distances of about 500 m the correlation is reduced to near zero by additional intrusions of thick packets of water with variable vertical temperature gradients, while the temperature near the bottom is partly in counter-phase with the temperature at 1300 m, as can be expected when thermostads are a dominant feature in the variable temperature structure. The strongest example of such a low  $T$  gradient intrusion occurs between days 800 and 840 (10 March–19 April 2006). In that sub-period the 2.5 and 3.0 °C isotherms move downwards, while the 3.5 and 4.0 °C isotherms move upwards, all over a vertical distance of over 100 m (Fig. 10). Apparently a deep thermostad with a low vertical stability, centred around 1700 m, passed Lifamatola Passage around day 822 (1 April 2006). Such a thick thermostad may have dynamic consequences for the deep flow, since it is probably also connected with changing horizontal density gradients. Evidence for this hypothesis can be seen in the

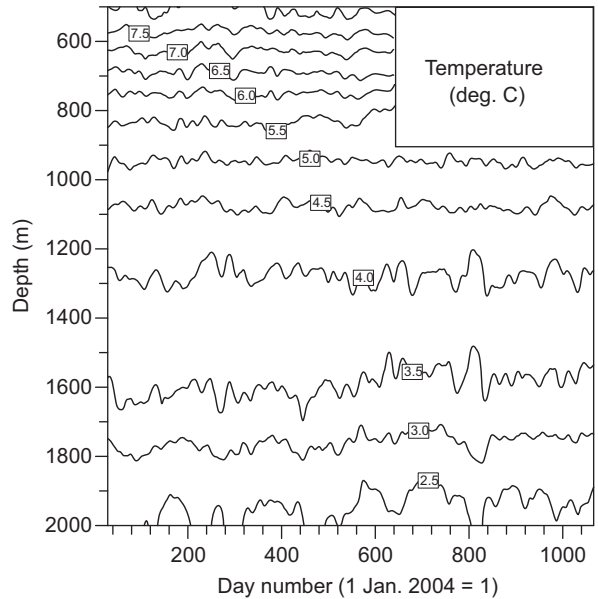


**Fig. 10.** Time–depth section of the temperature measured with the temperature sensors on the mooring. The signal was smoothed with a low-pass filter with a width of 14 days to remove the tidal contributions to the temporal variability.

velocity already at 1500 (Fig. 3), which shows a current reversal around that same date.

One may question whether the thermostad is formed locally, or whether it is advected from elsewhere. The thermostad around 1 April 2006 lasted at least 30 days, an earlier thermostad in October 2005 about 26 days. During these periods no particularly strong tides or other phenomena were observed, which may be responsible for local mixing over the sill as the cause of the occurrence of the thermostad. At the centre of the thermostad at a depth of 1700 m, the passage has a width of only about 14 km. During the 30 days of its occurrence, the mean down-channel velocity at 1700 m was 8 cm/s, suggesting an along-channel size of about 220 km. Apart from the effects of the convergence and divergence of the thermostad as it passes the narrow Lifamatola sill, these rough estimates

show that the thermostat was much longer than the width of the channel. This suggests that the thermostat was advected from the Maluku Sea to the Lifamatola sill. The cause of the formation of such deep thermostads upstream of the passage remains uncertain yet. The relatively large size of the thermostat in the along-flow direction ensures that the change of the pressure gradient due to the presence of a thermostat probably extends over the whole Lifamatola sill, and thereby influences the whole deep overflow.

## 6. Transports through Lifamatola Passage

With the velocity data, obtained from the moorings, we can calculate the volume transport across a section that runs perpendicular to the mean along-channel deep flow in the direction of 219°. The endpoints of that section are given in Table 2. The section runs from a ridge, extending northwestwards from Obimayor (depth 1090 m) across the deep channel in the Lifamatola Passage (maximum depth ~2050 m) to a “shallow” platform east-southeast of Lifamatola (depth 1645 m). The width of this section is 36.2 km, while at 1750 m it is only 10.5 km wide, intersected by the bottom topography (Fig. 2b). For the calculation of the transport we assume that the measured velocity profile (Fig. 6) is representative for the vertical velocity structure across the whole section. For the levels below the deepest interpolated velocity level, 2000 m, we apply the 2000-m velocity. Given the narrow width of the deep channel at these levels, the effect of this, or any other extrapolation, is very small.

The along-channel volume transport  $Tr$  over the sill between the depth levels  $z_0$  and  $z_1$  has been computed

**Table 2**

Endpoints of the transport section, through which the transports are calculated.

Latitude	Longitude
1°39.90'S	127°05.14'E
1°55.07'S	126°52.81'E

from the profile of the velocity in the direction of 129° by the following integral:

$$Tr = \int_{z_0}^{z_1} V_{129^\circ} W(z) dz, \quad (1)$$

where  $W(z)$  is the depth-varying width of the channel. We have calculated the volume transports for the depth intervals 450–1250 m and from 1250 to the bottom, since the along-channel velocity profile in Fig. 6 suggests that in these depth intervals the current is, respectively, in the northwestern and southeastern direction. These depth intervals are well covered by velocity estimates for the second deployment period, but for the first deployment period, part of the data in these intervals are missing in all or part of the months in this period. In order to prevent a possible bias in the transport estimate due to missing data, we have to find a method to obtain a reliable approximation for the transport for the first deployment.

For the second deployment period, with a complete data coverage for both depth intervals, the deep transport below 1250 m has been derived from the 5-day running mean values of the interpolated along-channel velocity. The resulting transport time series varies from -0.8 to 5.2 Sv, with an average value of 2.7 Sv ( $\pm 1.3$  Sv stdev). This transport is nearly twice the transport value of 1.5 Sv derived by Van Aken et al. (1988). This is partly because their 3.5 months of observations gave lower velocity values (vA crosses in Fig. 6) than our 1.5-year deployment period, and partly because their estimate of the thickness of the overflow layer (460 m) from linear extrapolation was smaller. The best linear correlation between the volume transport and the velocity at a single level ( $R = 0.993$ ) is found at a depth of 1500 m. The time series at this level is also complete for the first deployment period. We have calculated the volume transport for this period from the velocity at 1500 m by means of the linear regression with the along-channel velocity at 1500 m, derived from the data in the second deployment period.

The thin full line in Fig. 11 shows that there exists a regular fortnightly variability of the transport through the Lifamatola Passage below 1250 m, probably connected with the Mf tidal component. However, application of a

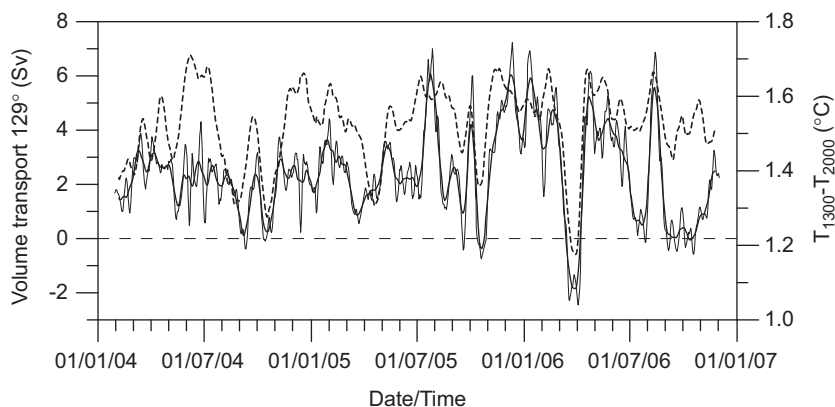


**Fig. 11.** Time series of the along-channel volume transport between 1250 m and the bottom in the direction 129°. Positive values are from the Maluku Sea southeastwards to the Seram Sea. The thin full line shows the 5-day running mean, the thick full line the 15-day running mean, where the fortnightly Mf tidal contribution is suppressed. The dashed line represents the 15-day running mean of the temperature difference between 1300 and 2000 dbar.

15-day running mean (thick full line in Fig. 11) effectively suppresses this tidal contribution. A peculiar phenomenon in the transport time series is the 22-day period around 1 April 2006, where the along-channel volume transport below 1250 m is negative. It appears that this is caused by the lowering of the zero-velocity interface, on average at  $\sim 1250$  m, to a level of nearly 1700 m, the deepest current reversal level observed in our records. This lowering coincides with the presence of the thermostat in the passage, centred around the same depth of 1700 m, as described above. A similar phenomenon, although less extreme, occurred around 20 October 2005. Apparently the vertical temperature gradient is related to the strength of the deep throughflow. The temperature difference between 1300 and 2000 m, assumed to be representative for the vertical temperature gradient in the deep throughflow and the presence of thermostads (Fig. 11, dashed line), shows a regular coincidence of high- or low-transport events with high or low temperature gradients.

The along-channel transport, derived from the 15-day running mean time series in Fig. 11, averaged over the whole near-3-year deployment period, amounts to 2.4 ( $\pm 1.5$  stdev) Sv, while the transport derived from the averaged profiles in Fig. 6 amounts to 2.5 Sv. Apparently the averaged velocity profile is not very sensitive to the bias caused by levels with incomplete data from the first deployment period.

In order to determine the average temperature of the deep throughflow below 1250 m, we have to determine the transport-weighted mean temperature. The transport-weighted temperature  $T_{TW}$  is defined as

$$T_{TW} = \frac{\int_{z_0}^{z_1} V_{129^\circ} T(z) W(z) dz}{Tr}, \quad (2)$$

where  $T(z)$  is the depth-dependent temperature, observed with the temperatures sensors in the mooring and  $Tr$  is defined in (1). When we calculate the long-term mean value of this  $T_{TW}$  with the 5-day-averaged time series of the along-channel velocity and temperature for the second deployment period, we obtain a mean transport-weighted temperature of 3.21 °C, while the use of mean vertical profiles of temperature and velocity for this period results in a mean temperature of 3.25 °C. Apparently the effects of any Reynolds terms in the total heat (temperature) transport are negative, but small, and can be ignored. For the total 34-month deployment period the mean temperature of the deep throughflow, derived from the long-term mean profiles of temperature and along-channel velocity, is 3.22 °C. The mean salinity of the deep throughflow, determined similarly, is 34.617, agreeing with the (near-homogeneous) salinity in the deep Banda Sea below 2000 m (34.615–34.620; Van Aken et al., 1988, 1991).

In the layer from 250 to 1250 m a significant mean velocity from the Maluku Sea to the Seram Sea is observed (Fig. 6). Given the increasing width of the Lifamatola Passage from 1250 to the sea surface, the assumption that the transport at these levels can be estimated from velocity measurements at a single mooring becomes questionable. But if we do this, the total volume transport in the 1000 m thick layer between 250 and 1250 m

amounts to  $-1.0 (\pm 1.1 \text{ stdev})$  Sv, which means a strongly varying, but on average northwestward, transport towards the Maluku Sea. An annual cycle of the northwestward velocity can be discerned only at 300 and 400 m depth, in counter-phase with the near-surface Ekman Transport at 7°S in the Banda Sea (Sprintall and Liu, 2005). If we assume that the residual velocity at 300 m extends to the sea surface, we arrive at a small residual northwestward transport in the upper 1250 m of 1.3 Sv. However, estimates of the current structure in Makassar Strait have shown that the vertical current structure in the upper 300 m of the Indonesian seas may show a considerable seasonal variability (Gordon et al., 2003a). These estimates of the transport above 1250 m, given above, are probably not very accurate, and should be interpreted with care.

## 7. Discussion

The data obtained with the INSTANT mooring in the Lifamatola Passage show that vigorous motion occurs in the deep channel across the sill. That motion consists of the residual flow, contributing to the deep ITF of cold water from the Pacific Ocean towards the Banda Sea and of vertically varying internal tides. Since the southern exits of the Banda Sea are all shallower than the sill in the Lifamatola Passage, this sill controls the deep throughflow from the Pacific to the Indian Ocean (Gordon et al., 2003b).

In the tidal motion the diurnal tides  $K_1$  and  $O_1$  are dominant, although Wyrтки (1961) has reported that in the sea areas around Sulawesi, also in the Lifamatola Passage, the surface tide is mixed, but prevailing semi-diurnal. Apparently the mooring was not intersected directly by a semi-diurnal internal tidal wave beam. Generation of (lower-frequency) diurnal internal tides by interaction of the barotropic tide and topography in a stratified sea requires a smaller critical bottom slope than the generation of the (higher-frequency) semi-diurnal internal tides, while a propagating diurnal internal wave beam will also follow a less-steep path than the semi-diurnal tide (Gill, 1982). The steeper critical bottom slope is probably found deeper on the sill, at a larger distance from the mooring near the top of the sill, than the smaller slope, where diurnal internal tides are generated. The shorter distance to the critical slope combined with the less-steep wave beams will favour the diurnal tide to reach the mooring. These frequency-dependent differences in generation areas and wave propagation may explain the observed local dominance of the diurnal internal tides over the sill.

We can assume that the strong tidal variation of the near-bottom temperature and salinity, measured during the second deployment period (Fig. 8), is caused mainly by vertical tidal motion of the isotherms and isohalines. From the temperature signal and the mean vertical gradient of the potential temperature we then derive the standard deviation of the vertical excursion to be 156 m. The standard deviation of the vertical excursion, derived from the variations of the salinity, is 144 m, within 10% a similar

value. This value agrees with the large vertical motion of the isotherms presented for periods of 4 days by Van Aken et al. (1988), who show depth variations of isotherms (peak–trough) of about 400 m (their Fig. 8). This result also indicates that it is hard to derive the near-bottom vertical stratification from only a few CTD casts. More detailed modelling studies on the generation of internal tides, in combination with resulting generation of turbulent mixing in a general circulation model, like those carried out by Koch-Larrouy et al. (2007), may shed light on the question where and how internal tides contribute to the enhanced turbulent mixing in the deep Indonesian seas, derived by Van Aken et al. (1988, 1991).

The main transport in the Lifamatola Passage, responsible for the cold part of the ITF and the ventilation of the deep Banda Sea, appears to be concentrated in the lower layer of the water column below 1250 m (Fig. 6), with a velocity maximum of over 65 cm/s at ~70 m above the bottom. The observed downward decrease of the velocity below that level is probably related to friction effects in the near-bottom layers. The long-term mean volume transport in this cold ITF, estimated in different ways, amounts to 2.4–2.5 Sv for the total 34-month deployment period. This is nearly 60% higher than the volume transport of 1.5 Sv, derived from a much shorter deployment period of only 3.5 months, reported by Van Aken et al. (1988). This difference is not necessarily connected with long-term changes. From our 34-month transport record (Fig. 11) one can derive that on average 15% of the 3-month-average transports have a magnitude of 1.5 Sv or less. It can be concluded that the relatively low transport, reported by Van Aken et al. (1988), is not really a rare event.

The time series of the cold transport, shown in Fig. 11, shows an occasionally strong variation with a time scale of about 1 month. It has been shown that the negative-transport event around 1 April 2006 coincided with the presence of a deep hydrographic feature centred at 1700 m, characterized by a strongly reduced vertical temperature gradient, a thermostad. Below 1700 m the residual flow was then still directed towards the Seram Sea, with near-bottom velocities at 1950 m of well over 40 cm/s. The negative correlation between the temperature at 1950 and 1300 m suggests that variations in the vertical temperature gradient, as they occur in a thermostad, are a dominant feature below 1250 m. To analyze whether the relation between the presence of a thermostad in the lowest 750 m and the reduction of the deep overflow can be generalized, we have determined the correlation between the 15-day running mean of the volume transport below 1250 m and the temperature difference between 1300 and 2000 m. The resulting correlation is 0.62. Apparently, deep thermostads are encountered regularly in the Lifamatola Passage, and they cause a decrease in the volume transport. The source and dynamics of these deep features are unknown yet, but the coincidence of the strong thermostad at 1700 m with the low-transport event, as well as the significant correlation between transport and vertical temperature gradient, suggests that both are related.

The long-term averaged deep transport derived from our data, 2.5 Sv, is considerably smaller than the southward transport between 740 and 1500 m of ~7 Sv, derived by Luick and Cresswell (2001) for a section in the Maluku Sea between Sulawesi and Halmahera. The transport over a similar depth interval derived from our mooring data, is –0.3 Sv, directed to the northwest. This large contrast clearly indicates, as was already suggested by Luick and Cresswell (2001), that the assumption that the averaged current data from a mooring at the extreme western side of a 230 km wide section are representative for the entire width of this passage is indeed doubtful. Representative deep current observations are more likely obtained for our section of only 36 km wide, although even in this case the lateral homogeneity is still an assumption, not yet a proven fact. At shallower levels of, e.g., 500 m the cross-channel distance between the isobaths in the Lifamatola Passage is about one third of the section used by Luick and Cresswell (2001), but even over such a distance it is doubtful that the use of a single current meter mooring will produce an accurate estimate of the shallow transport.

The inflow of cold water through the Lifamatola Passage, in addition to the main ITF branch through the Makassar Strait, influences not only the volume budget of the ITF but also the heat transport. The existing transport estimate of the strength of the warm Makassar Strait branch based on the Arlindo Experiment (Gordon et al., 1999) is 9.3 Sv. The deep inflow through Lifamatola Passage, presented here, adds over 25% of cold water to this estimate. Vranes et al. (2002) derived the transport-weighted temperature in Makassar Strait by four different methods and found a mean value of 14.6 ( $\pm 1.8$  stdev) °C. If we combine these (non-contemporary!) results with the mean transport and transport-weighted temperature from the deep transport in Lifamatola Passage (2.5 Sv and 3.2 °C), we arrive at a total northern inflow of the ITF into the Indonesian seas of 11.8 Sv, with a transport-weighted mean temperature of about 12.2 °C. This temperature is considerably lower than the temperature estimates from the past of well over 20 °C (Gordon et al., 2003). When considering these results, one has to be aware that these results are obtained by putting together data collected from different experiments, carried out over different years. But new data from all the different contemporary experiments of the INSTANT programme may lead to a thorough revision of the heat budget of the ITF.

The 2.5 Sv cold deep water entering the Banda Sea system with a mean temperature of 3.2 °C rises there to shallower levels before it can leave for the Indian Ocean through the passages between the lesser Sunda Islands or around Timor. According to Gordon et al. (2003b) this deep water leaves the Banda Sea after upwelling to depths between 1300 and 680 m or shallower, before it leaves for the Indian Ocean. The deeper part of this throughflow occurs through the Timor Passage and Ombai Strait (T and O in Fig. 1). This agrees quite well with the available ETOPO-2 2'  $\times$  2' resolution topographic data set (Smith and Sandwell, 1997). Preliminary direct transport estimates of the throughflow entering the Indian Ocean, derived from other parts of the INSTANT experiment,

suggest a deep maximum in this throughflow at  $\sim 1000$  m depth (Sprintall et al., 2009). At that level the Banda Sea has a mean temperature of  $\sim 5.0^\circ\text{C}$  (Van Aken et al., 1988). The heat transported by 2.5 Sv at  $5^\circ\text{C}$  is larger than that by the same volume transport in the Lifamatola Passage at  $3.2^\circ\text{C}$ . This implies that the heat flux of the deep throughflow in the Banda Sea is divergent, and extra heat has to be supplied to warm the upwelling cold water (Munk, 1966; Van Aken et al., 1991). This heat source is supplied by turbulent mixing with the overlying water. Given that the surface of the Banda Sea is  $\sim 6.7 \times 10^{11} \text{ m}^2$ , and the specific heat of sea water is about  $4000 \text{ J/kg}^\circ\text{C}$ , the downward turbulent heat flux in the Banda Sea at a level of 1000 m should supply  $28 \text{ W/km}^2$  to support the divergent advective heat flux. If the cold throughflow rises up to the shallower level of 500 m, where the mean temperature is  $8^\circ\text{C}$  (Van Aken et al., 1988), a downward turbulent heat flux of  $74 \text{ W/m}^2$  is required. Upwelling of the cold ITF to even shallower and warmer levels needs even larger heat inputs. This heat is supplied by the cooling of the overlying water, and ultimately by cooling of the atmosphere in Indonesia. Apparently, maintenance of the deep throughflow through the Lifamatola Passage may have a considerable influence on the local climate, of the same order of magnitude as the heat flux sustained by the throughflow of thermocline water ( $\sim 100 \text{ W/m}^2$ ) proposed by Gordon (1986).

The downward turbulent heat flux in the water column is balanced by the upward advective heat flux. Using the vertical advection–diffusion model, proposed by Munk (1966), and using a deep transport estimate of 1 Sv, Van Aken et al. (1988, 1991) were able to estimate the turbulent diffusion coefficient in the Banda Sea to be  $9 \times 10^{-4} \text{ m}^2/\text{s}$ . Given a known temperature stratification in the Banda Sea, the turbulent diffusion coefficient derived from Munk's model is proportional to the vertical upwelling velocity, which is in its turn proportional to the deep inflow of cold water. With our new estimate of an inflow of 2.5 Sv, this leads to an estimate of about  $2.2 \times 10^{-3} \text{ m}^2/\text{s}$ , more than a factor of 20 higher than the generally accepted canonical value of  $10^{-4} \text{ m}^2/\text{s}$  for the world ocean (Gargett, 1984). Apparently, the strong internal tides in the Banda Sea contribute strongly to the turbulent energy budget responsible for the maintenance of the downward turbulent heat flux and the considerable mixing in the Banda Sea (Van Aken et al., 1988; Koch-Larrouy et al., 2007).

When more results from the INSTANT programme become available, it is likely that a more reliable budget for the ITF of mass, heat, and freshwater than currently available can be produced. These will form a benchmark for model simulations of the interocean exchange between the Pacific and Indian Oceans and are expected to boost our understanding of these processes for the oceanic climate.

### Acknowledgements

We thank the captains and crew of the Baruna Jaya I of the Indonesian Agency for Research and Application of

Technology (BPPT) and the technicians and scientists from the Agency for Marine and Fisheries Research (BRKP) for their support during the research cruises. Many Indonesian students also participated in the three cruises. Theo Hillebrand and Sven Ober prepared and serviced the instruments, while Marcel Bakker, Jack Schilling, and Leon Wuijs were responsible for the construction and handling of the mooring, and Kees Veth replaced HMvA during the last cruise. Funding for the mooring equipment was received from the Netherlands Foundation for Scientific Research (NWO) via the LOCO investment programme, and via the IMAU of Utrecht University from the COACH International Research School. Ship time of the RV Baruna Jaya I was made available by the BRKP.

### References

- Broecker, W.S., Patzert, W.C., Toggweiler, J.R., Stuiver, M., 1986. Hydrography, chemistry, and radioisotopes in the southeast Asian waters. *Journal of Geophysical Research* 91, 14,345–14,354.
- Emery, W.J., Thomson, R.E., 1997. *Data Analysis Methods in Physical Oceanography*. Pergamon, Oxford, p. 634.
- Ffield, A., Robertson, R., 2005. Indonesian seas finestructure variability. *Oceanography* 18, 108–111.
- Gargett, A.E., 1984. Vertical eddy diffusivity in the ocean interior. *Dynamics of Atmospheres and Oceans* 42, 359–393.
- Gill, A.E., 1982. *Atmosphere–Ocean Dynamics*. Academic Press, London, p. 662.
- Gordon, A.L., 1986. Interocean exchange of thermocline water. *Journal of Geophysical Research* 91, 5037–5046.
- Gordon, A.L., Fine, R.A., 1996. Pathways of water between the Pacific and Indian oceans in the Indonesian sea. *Nature* 379, 146–149.
- Gordon, A.L., Susanto, R.D., Ffield, A., 1999. Throughflow within Makassar Strait. *Geophysical Research Letters* 26, 3325–3328.
- Gordon, A.L., Susanto, R.D., Vranes, K., 2003a. Cool Indonesian throughflow as a consequence of restricted surface layer flow. *Nature* 425, 824–828.
- Gordon, A.L., Giulivi, C.F., Ilahude, A.G., 2003b. Deep topographic barriers within the Indonesian Seas. *Deep-Sea Research II* 50, 2205–2228.
- Koch-Larrouy, A., Madec, G., Bouruet-Aubertot, P., Gerkema, T., Bessières, L., Molcard, R., 2007. On the transformation of Pacific water into Indonesian throughflow water by internal tidal mixing. *Geophysical Research Letters* 34, L04604.
- Lek, L., 1938. The Snellius Expedition in the eastern part of the East Indian Archipelago 1929–1930. Vol. II: Oceanographic results. Part 3: Die Ergebnisse der Strom- und Serimessungen (in German).
- Luick, J.L., Cresswell, G.R., 2001. Current measurements in the Maluku Sea. *Journal of Geophysical Research* 106, 13953–13958.
- Molcard, R., Fieux, M., Swallow, J.C., Ilahude, A.G., Banjarnahor, J., 1994. Low frequency variability of the currents in Indonesian channels (Savu-Roti and Roti-Ashmore Reef). *Deep-Sea Research I* 41, 1643–1661.
- Molcard, R., Fieux, M., Ilahude, A.G., 1996. The Indo-Pacific throughflow in the Timor Passage. *Journal of Geophysical Research* 101, 12,411–12,420.
- Molcard, R., Fieux, M., Syamsudin, F., 2001. The throughflow within Ombai Strait. *Deep-Sea Research I* 48, 1237–1253.
- Munk, W.H., 1966. Abyssal recipes. *Deep-Sea Research* 13, 707–730.
- Murray, S.P., Arief, D., 1988. Throughflow into the Indian Ocean through the Lombok Strait, January 1985–January 1986. *Nature* 333, 444–447.
- Pandey, V.K., Bhatt, V., Pandey, A.C., Das, I.M.L., 2007. Impact of Indonesian throughflow blockage on the Southern Indian Ocean. *Current Science* 93, 399–406.
- Schneider, N., 1998. The Indonesian throughflow and the global climate system. *Journal of Climate* 11, 676–689.
- Smith, W.H.F., Sandwell, D.T., 1997. Global sea floor topography from satellite altimetry and ship depth soundings. *Science* 277, 1956–1962.
- Sprintall, J., Wijffels, S., Gordon, A.L., Ffield, A., Molcard, R., Susanto, R.D., Soesilo, I., Spaheluwakan, J., Surachman, Y., van Aken, H.M., 2004. INSTANT, a new international array to measure the Indonesian throughflow. *EOS, Transactions, American Geophysical Union* 85 (39), 369–376.

- Sprintall, J., Wijffels, S.E., Molcard, R., Jaya, I., 2009. Direct estimates of the Indonesian Throughflow entering the Indian Ocean: 2004–2006. *Journal of Geophysical Research*, in press.
- Sprintall, J., Liu, W.T., 2005. Ekman mass and heat transport in the Indonesian seas. *Oceanography* 18 (4), 88–97.
- Tomczak, M., Godfrey, J.S., 1994. *Regional Oceanography, and Introduction*. Pergamon, Oxford, p. 422.
- Van Aken, H.M., Punjanan, J., Saimima, S., 1988. Physical aspects of the flushing of the East Indonesian basins. *Netherlands Journal of Sea Research* 22, 315–339.
- Van Aken, H.M., van Bennekom, A.J., Mook, W., Postma, H., 1991. Application of Munk's abyssal recipes to tracer distributions in the deep waters of the South Banda Sea. *Oceanologica Acta* 14, 151–162.
- Van Riel, P.M., 1956. The Snellius Expedition in the eastern part of the East Indian Archipelago 1929–1930. Vol. II: Oceanographic results. Part 5: The bottom water. Ch. II: Temperature.
- Vranes, K., Gordon, A.L., Field, A., 2002. The heat transport of the Indonesian Throughflow and implications for the Indian Ocean heat budget. *Deep-Sea Research II* 49, 1391–1410.
- Wajsowicz, R.C., Schneider, E.K., 2001. The Indonesian throughflow's effect on global climate determined from the COLA coupled climate model. *Journal of Climate* 14, 3029–3042.
- Wyrtki, K., 1961. NAGA Report. Vol. 2: Scientific results of marine investigations of the South China Sea and the Gulf of Thailand 1959–1961. Scripps Institution of Oceanography, La Jolla, p. 195.